HHS Public Access

Author manuscript

*Neuroimage*. Author manuscript; available in PMC 2021 April 09.

Published in final edited form as:

*Neuroimage*. 2021 February 15; 227: 117680. doi:10.1016/j.neuroimage.2020.117680.

# Co-activation patterns across multiple tasks reveal robust anti-correlated functional networks

**Meiling Li**[a,1], **Louisa Dahmani**[a,b,1], **Danhong Wang**[a], **Jianxun Ren**[a], **Sophia Stocklein**[c], **Yuanxiang Lin**[d], **Guoming Luan**[e], **Zhiqiang Zhang**[f], **Guangming Lu**[f], **Fanziska Galiè**[a,c], **Ying Han**[g], **Alvaro Pascual-Leone**[h], **Meiyun Wang**[b,*], **Michael D. Fox**[a,i,j], **Hesheng Liu**[a,k,l]

[a]Athinoula A. Martinos Center for Biomedical Imaging, Department of Radiology, Massachusetts General Hospital, Harvard Medical School, Charlestown, MA, USA

[b]Department of Medical Imaging, Zhengzhou University People Hospital & Henan Provincial People's Hospital, Zhengzhou, Henan, China

[c]Department of Radiology, Ludwig Maximilian University of Munich, Munich, Germany

[d]Department of Neurosurgery, First Affiliated Hospital of Fujian Medical University, Fuzhou, China

[e]Department of Neurosurgery, Comprehensive Epilepsy Center, Sanbo Brain Hospital, Capital Medical University, Beijing, China

[f]Department of Medical Imaging, Jinling Hospital, Clinical School of Medical College, Nanjing University, Nanjing, China

[g]Department of Neurology, Xuanwu Hospital of Capital Medical University, Beijing, China

[h]Marcus Institute for Aging Research, Hebrew SeniorLife, Harvard Medical School, Boston, MA, USA

[i]Center for Brain Circuit Therapeutics, Departments of Neurology, Psychiatry, and Radiology, Brigham and Women's Hospital, Harvard Medical School, Boston, MA, USA

[j]Department of Neurology, Massachusetts General Hospital, Harvard Medical School, Boston, MA, USA

[k]Beijing Institute for Brain Disorders, Capital Medical University, Beijing, China



*Corresponding author. mywang@ha.edu.cn (M. Wang).

[1]Contributed equally.

Author contributions

H.L., M.L. and M.W. conceived the study; M.L. and H.L. designed the algorithm; M.L., L.D., D.W., J.R., and F.G. performed the analyses with support from S.S. and M.D.F.; M.W., A.P.L, Y.H., Guo.L., Z.Z., Gua.L., and Y.L. provided support and guidance with data interpretation. L.D., H.L., M.L., and F.G. wrote the manuscript with contribution from S.S. and M.D.F. All authors commented on the manuscript.

Data and code availability

The dataset HCP were publicly available through the NIH Human Connectome Project (https://www.humanconnectome.org/). MATLAB codes that support the findings of this study are available from http://nmr.mgh.harvard.edu/bid/DownLoad.html

Declaration of Competing Interest

The authors declare no competing financial interests.

Supplementary materials

Supplementary material associated with this article can be found, in the online version, at doi: 10.1016/j.neuroimage.2020.117680.

[l]Department of Neuroscience, Medical University of South Carolina, Charleston, SC, USA

## Abstract

Whether antagonistic brain states constitute a fundamental principle of human brain organization has been debated over the past decade. Some argue that intrinsically anti-correlated brain networks in resting-state functional connectivity are an artifact of preprocessing. Others argue that anti-correlations are biologically meaningful predictors of how the brain will respond to different stimuli. Here, we investigated the co-activation patterns across the whole brain in various tasks and test whether brain regions demonstrate anti-correlated activity similar to those observed at rest. We examined brain activity in 47 task contrasts from the Human Connectome Project ($N$ = 680) and found robust antagonistic interactions between networks. Regions of the default network exhibited the highest degree of cortex-wide negative connectivity. The negative co-activation patterns across tasks showed good correspondence to that derived from resting-state data processed with global signal regression (GSR). Interestingly, GSR-processed resting-state data was a significantly better predictor of task-induced modulation than data processed without GSR. Finally, in a cohort of 25 patients with depression, we found that task-based anti-correlations between the dorsolateral prefrontal cortex (DLPFC) and subgenual anterior cingulate cortex were associated with clinical efficacy of transcranial magnetic stimulation therapy targeting the DLPFC. Overall, our findings indicate that anti-correlations are a biologically meaningful phenomenon and may reflect an important principle of functional brain organization.

### Keywords

Anti-correlations; Functional connectivity; Task fMRI; Global signal regression; Transcranial magnetic stimulation

## 1. Introduction

Anti-correlations in functional activity among brain networks have been a subject of debate for the last decade. In 2005, two reports introduced the concept of anti-correlated networks as a fundamental principle of functional brain organization (Fox et al., 2005; Fransson, 2005). They showed, using resting-state functional Magnetic Resonance Imaging (fMRI), that two large-scale brain networks, the default network (DN) and dorsal attention network (DAN), exhibit a competitive interaction. This study underlined a dichotomy between these two networks, whereby their spontaneous activity is anticorrelated, i.e. their activity moves in opposite directions. Since then, anti-correlations among various networks have been reported (Chai et al., 2012; Esposito et al., 2018; Fransson, 2005; Raichle, 2015). However, in 2009, Murphy et al. (2009) demonstrated that global signal regression (GSR), an MRI preprocessing step commonly used in resting-state fMRI studies, mathematically mandates anti-correlations. This raised the possibility that the anti-correlations observed among resting-state networks could be artifactual. This concern was partially mitigated by the finding that anti-correlations between the DN and DAN could be detected even without GSR (Chai et al., 2012). Recent studies further showed that anti-correlations may have a meaningful neurobiological basis, as anti-correlations were predictive of depressive symptom improvement following an intervention (Fox et al., 2014, 2012a; Weigand et al.,

2018), and could be used to link spatially heterogeneous brain lesions to homogeneous symptoms in different individuals (Boes et al., 2015; Fox, 2018). As an example, anti-correlations between repetitive Transcranial Magnetic Stimulation (rTMS) sites in the dorsolateral prefrontal cortex (DLPFC) and the subgenual anterior cingulate cortex (sgACC) were associated with greater therapeutic efficacy in a cohort of patients with major depressive disorder (Cash et al., 2019; Weigand et al., 2018), indicating that anti-correlations may be important characteristics of functional brain organization that track with patients' symptoms.

The global signal is defined as the time series of the average signal intensity across all voxels within the brain (Zarahn et al., 1997). GSR is a preprocessing technique that eliminates global signal fluctuations through a linear regression, and has a number of advantages and disadvantages. In terms of advantages, GSR is efficacious in removing non-neural signals, including motion artifacts, physiological noise (cardiac and respiratory activity), and low-frequency scanner drift (Ciric et al., 2017; Liu et al., 2017; Parkes et al., 2018; Power et al., 2017b; Yan et al., 2013). Likely as a result of this noise removal, GSR has been shown to enhance the neuroanatomical specificity of positive correlations and the detection of anticorrelations (Fox et al., 2009; Weissenbacher et al., 2009), and to increase functional connectivity-behavior relationships (Li et al., 2019b).

On the other hand, a prominent disadvantage of GSR is that it exaggerates or creates spurious anticorrelations. It does so (Yan et al., 2013) by zero-centering correlations for every voxel across all brain voxels, which inherently creates anti-correlations as the mean is centered around zero and correlations are distributed equally in the negative and positive ranges (Fox et al., 2009; Murphy et al., 2009). GSR may also exacerbate motion artifacts in short-range relative to long-range functional connections (Ciric et al., 2017; Parkes et al., 2018), and was shown to only be effective in removing specific widespread signal deflections, leaving others largely untouched (Aquino et al., 2020). GSR has the additional detriment of removing at least some neural signal (Liu et al., 2017). Indeed, there is evidence that there are neural origins to the global signal, as it is associated with spontaneous fluctuations in the local field potential (Schölvinck et al., 2010), vigilance (Wong et al., 2013), arousal (Chang et al., 2016; Liu et al., 2018), baseline brain metabolism (Thompson et al., 2016), and time of day (Orban et al., 2020). Additionally, pharmacological inactivation of the monkey basal forebrain, which is an important source of cholinergic and non-cholinergic input to the cortex (Zaborszky et al., 2015), led to a large region-specific suppression of global signal components (Turchi et al., 2018). A recent report has also shown that individual differences in the topology of the global signal are associated with various cognitive and behavioral measures (Li et al., 2019a). Therefore, while GSR is useful in the removal of non-neural signals, it has clear disadvantages in its inherent bias towards anti-correlations and in its partial removal of neural signal, some of which is individual-specific and behaviorally relevant. Murphy and Fox (2017) have made progress towards a consensus on the use of GSR, describing that it offers value as a way to enhance the detection of brain-behavior relationships in some situations, but that care should be taken in the interpretation of these anti-correlations.

In the current study, we explored the opposing relationship among functional networks using a variety of task conditions spanning different cognitive domains in a large sample from the Human Connectome Project (HCP; $N = 680$ selected from the S900 release). We concatenated task activation maps as if they were signals observed at different time points, and then investigated whether two brain regions consistently show anti-correlated activity across different tasks. Unlike in resting-state fMRI analysis, this task-based correlation analysis bypassed the need to remove the global mean signal at each "time point". To gain a deeper understanding of how GSR biases the observation of anti-correlations in resting-state data, we compared our task coactivation-based anti-correlations to the anti-correlations observed in resting-state data preprocessed with and without GSR. We then explored the number of negative functional connections across the whole brain and examined their spatial distribution across brain states (task performance vs. resting-state) and across preprocessing techniques (with and without GSR). Finally, we revisited the question of whether anti-correlations are informative in a clinical context. We analyzed data from a previous report (Weigand et al., 2018) and investigated whether both task coactivation-based and resting-state anti-correlations can track with therapeutic efficacy of non-invasive brain stimulation in a sample of 25 patients with medically-intractable depression.

## 2. Methods

### 2.1. Participants and data acquisition

**Dataset I.—***Dataset I.* The primary cohort consisted of 680 participants (375 women; 305 men) from the Human Connectome Project (HCP) S900 release based on the following inclusion criteria: 1) data of four resting-state fMRI sessions and seven task fMRI sessions were available; 2) each resting-state fMRI session had 1200 time points; 3) mean relative head displacement of each resting-state session was smaller than 0.15 mm (Shen et al., 2017). Functional data were obtained using a gradient echo-planar pulse sequence with a temporal resolution of 0.72 s and 2 mm isotropic spatial resolution. Structural T1-weighted and T2-weighted images were acquired with 0.7 mm isotropic resolution and B0 field mapping was also acquired to aid in correcting EPI distortions. Written informed consent was obtained from each participant in accordance with relevant guidelines and regulations approved by the local institutional review board at Washington University in St. Louis (IRB # 201,204,036). Detailed descriptions about the dataset have previously been reported (Barch et al., 2013; Van Essen et al., 2013, 2012).

**Dataset II.—**The second dataset included 25 patients with medication-resistant major depressive disorder (17 women; 8 men) with a mean age of 54.8 years (SD = 9.9, range = 28–67 years of age), which was described in a previous study (Weigand et al., 2018). The mean Beck Depression Inventory (BDI) score at baseline was 38.6 (SD = 9.3) and significantly decreased to 21.2 (SD = 13.0) after the course of rTMS treatment ($t(24) = 10.05$, $p < 0.0001$). This cohort is described in more detail in Weigand et al. (2018) (see Boston cohort). The 25 left DLPFC stimulation sites were identified individually at average Montreal Neurological Institute (MNI) coordinates: $x = -33 \pm 7$, $y = 30 \pm 9$, and $z = 50 \pm 9$ using the 5-cm approach, and the rTMS sites used in the present study were created by centering a 12 mm radius sphere at the coordinates of each stimulation site. To perform

connectivity analyses using a surface coordinate system, we registered the 25 rTMS sites from MNI space to fsaverage space using the RF-ANTS (Registration Fusion-Advanced Normalization Tools) mapping method (Wu et al., 2018). Then, using the connectome workbench command, we registered the rTMS sites from fsaverage to the fsLR coordinate system. Written informed consent was obtained from each participant in accordance with relevant guidelines and regulations approved by the Beth Israel Deaconess Medical Center's Internal Review Board (Weigand et al. (2018).

### 2.2. HCP tasks

The task fMRI data included 47 unique (excluding the paired opposite contrasts) contrast activation maps from seven cognitive domains, including working memory (WM), gambling (Gambling), motor (Motor), language (Language), social cognition (Social), relational processing (Relational), and emotional processing (Emotion), briefly described below. These tasks are described in more detail in Barch et al. (2013).

**Motor task.—**Participants executed cued movements with their hand, foot, or tongue. In a control condition, they fixated onto a crosshair in the middle of the screen.

**Language task.—**The language task was comprised of a Story and a Math condition. In the story condition, participants listened to stories and had to indicate the topic of the story, choosing between two responses. In the math condition, participants solved simple mathematical problems (addition and subtraction) and indicated which of two answers was correct.

**Working memory task.—**Participants were shown blocks of different stimuli (scenes, faces, tools, or body parts) as well as blocks where they fixated on the screen. Participants indicated whether the stimulus was the same as that shown two stimulus presentations prior (2-back task), or whether it matched the immediately preceding stimulus (0-back task).

**Gambling task.—**Participants were shown a mystery card and guessed whether the number on the card was smaller or larger than five. Money was used as an incentive for correct guesses. The numbers on the cards were then revealed, but were first manipulated to produce mostly correct guesses or mostly wrong guesses. This ensured approximately equal proportions of correct and wrong answers, enabling all participants to receive the same reward.

**Relational processing task.—**Participants were presented with one pair of objects at the top of the screen and one pair of objects at the bottom of the screen. In an experimental condition, participants decided on which attribute the top objects differed (shape or texture), and whether the bottom pair of objects differed in the same fashion. In a control condition, participants were presented a pair of objects at the top of the screen and a single object at the bottom of the screen, and decided whether the bottom object matched either of the top objects on a given attribute.

**Social cognition task.—**This task consisted in a theory of mind (ToM) task, where participants viewed video clips of shapes that were interacting or moving in a random

fashion. At the end of each video, participants indicated whether the objects had exhibited a social-like interaction.

**Emotion processing task.—**Participants were shown a face at the top of the screen and two faces at the bottom of the screen. Participants indicates which of the two bottom faces matched the emotional expression of the top face. Faces displayed either fearful or angry expressions. The control condition involved shapes instead of faces, and participants indicated which of the bottom shapes matched the top shape.

The contrasts used for each task are presented in Table 1.

## 2.3. MRI data analysis

**Dataset I.—**Resting-state HCP data, preprocessed using the ICA-FIX denoising approach, were downloaded from the HCP database (Glasser et al., 2016; Smith et al., 2013). As recent studies have reported that multiple noise components still exist and undermine functional connectivity-behavior relationships (Dubois et al., 2018; Siegel et al., 2017), we further preprocessed the data to decrease noise using an in-house pipeline. It should be noted that the original HCP preprocessing pipeline does not include GSR. In this study, we compared analyses with and without GSR applied in the preprocessing stage. The in-house GSR processing pipeline that we applied to the ICA-FIX-processed data included the following steps: 1) demeaning and detrending; 2) regression of motion and motion derivatives; 3) regression of the average cerebrospinal fluid signal, average white matter signal, and average whole-brain signal; and 4) band-pass filtering between 0.01 and 0.08 Hz. The non-GSR preprocessing pipeline was the same, except we omitted the average whole-brain signal from the regression in Step 3. We note that the complete preprocessing pipeline included two motion regressions: one as part of the HCP's ICA-FIX pipeline (Glasser et al., 2016), and the other as part of our in-house preprocessing pipeline, which is normally applied to raw data (rather than data that was already preprocessed). We assessed whether the second motion regression had an impact on the data (see Results section).

Task fMRI data were already preprocessed and analyzed by the HCP (Barch et al., 2013; Woolrich et al., 2001), and did not involve GSR. Task activation maps with 4 mm Gaussian smoothing were used and we did not perform any additional preprocessing on the task fMRI data. To extract task activation values, we used beta values (task effect size) to estimate the BOLD signal changes induced by different conditions and tasks (Glasser et al., 2016). For all analyses, we used data resampled to the 32k_fs_LR surface space (Kong et al., 2019).

**2.3.1. FMRI bold activity and functional connectivity:** The schematic diagram of the analyses and results are shown in Fig. S1. To investigate the co-activation patterns across the whole brain in various tasks, we first concatenated the 47 task contrasts available from the HCP. Specifically, we used 13 contrasts from the motor task, 3 contrasts from the language task, 19 contrasts from the working memory task, 3 contrasts from the gambling task, 3 contrasts from the relational task, 3 contrasts from the social cognition task, and 3 contrasts from the emotion task. Table 1 describes each specific contrast. The concatenated contrasts in each participant were treated similar to a time series, where each contrast corresponded to a single frame.

To visually check activity with positively or negatively correlated fluctuations during task performance, we plotted the 47 beta values for each vertex within three seeds: the posterior cingulate cortex (PCC), middle temporal gyrus (MTG), and frontal eye field (FEF), and averaged beta values across all vertices within each given seed region. To verify whether the positive and negative correlations in task co-activation maps resemble those usually reported for functional connectivity data in the resting-state literature, we generated a correlation map (Pearson's $r$ coefficient) between the PCC seed and every other cortical vertex using the concatenated 47 beta values. We generated maps for a randomly chosen HCP participant and for the HCP cohort as a whole, where individual correlation maps were averaged across all participants. For the population maps, we converted the $r$ coefficients to $z$ scores, at the individual level, using Fisher's $z$ transformation, then generated group-averaged $z$ maps, which we then reconverted back to $r$ to produce correlation maps. The schematic diagram of this analysis is shown in Fig. S1A.

To further investigate whether brain regions demonstrate similar anti-correlated activity during task performance and at rest, we examined co-activation patterns in the task fMRI data and functional connectivity derived from the resting-state fMRI data. We examined 8 seed regions, including 4 seeds from the DN: the PCC, medial prefrontal cortex (mPFC), posterior inferior parietal lobe (pIPL), and MTG, and 4 seeds from the DAN: middle temporal region (area MT+), superior parietal lobule (SPL), FEF, and inferior frontal junction (IFJ) (Fig. 2, top). These seeds were created by clustering the discrete patches in the DN and DAN from the 17 canonical networks (Yeo et al., 2011). For the task data, we calculated Pearson's correlations between the 47 beta values of each seed region (beta values were averaged across all vertices within that region) and those of every other vertex. For the resting-state fMRI data (GSR and non-GSR preprocessed), we concatenated the time series of all available sessions. For each seed region and participant, we averaged the times series of the vertices within the seed, calculated *Pearson's* correlations between the average time series and that of each of the other cortical vertices. Next, we determined which of GSR or non-GSR processed data yielded anti-correlation profiles that were more similar to task-based profiles. To do so, we binarized the connectivity profile of each seed according to the presence of anti-correlations. That is, positive correlations ($0 \leq r \leq 1$) were equated to 0, and all anti-correlations ($-1 \leq r < 0$) were equated to 1. We then calculated the Dice overlap of the binarized anti-correlation profile of each seed between the Task and Rest-no GSR conditions, and between the Task and Rest-GSR conditions, using the following formula:

$$Dice = \frac{2|x \cap y|}{|x| + |y|}$$

The Dice overlap indicates the extent of similarity between any two datasets. In this case, it returns the proportion of vertices that show anti-correlations with the seed in the two conditions being compared, within participants, over all anti-correlations present in the two datasets. The Dice coefficients were then averaged across participants, for each seed. To determine which resting-state data yielded anti-correlation profiles that were more similar to the task-based ones, we compared the averaged Dice coefficients using a paired $t$-test. The schematic diagram of this analysis is shown in Fig. S1B.

**2.3.2. Degree of anti-correlations and similarity in anti-correlation profiles:** To examine anti-correlations across the whole brain, we calculated the connectivity profile for each vertex, and investigated the degree of anti-correlations. Connectivity profile for each vertex was defined as the *Pearson's* correlations (co-activation for task fMRI and functional connectivity for resting-state fMRI) between a given vertex and all other 1483 vertices uniformly distributed on the 32k fs_LR surface (Kong et al., 2019). Specifically, the 1483 sparse vertex space was constructed by creating a sphere with 900 vertices (900 fs_LR surface) via workbench command ("-surface-create-sphere"), after which each vertex on the 900 fs_LR surface was matched to the nearest vertex on the 32k fs_LR surface. The degree of anti-correlations for each vertex was defined as the number of negative correlations in the connectivity profile, which quantifies the extent to which an area is competing with other areas in task or at rest. For each vertex, the degree of anti-correlations was averaged across participants. We also normalized the degree of anti-correlations using min-max normalization. We calculated these for all three conditions (Task, Rest-GSR, Rest-no GSR). The schematic diagram of this analysis is shown in Fig. S1C.

We additionally sought to compare the anti-correlation profiles across conditions and brain states at vertex-level on the whole brain. We first binarized the connectivity profile of each vertex according to the presence of anti-correlations. We then calculated the Dice overlap of the binarized anti-correlation profile of each vertex between the Task and Rest-no GSR conditions, and between the Task and Rest-GSR conditions. The Dice coefficient for each vertex was then averaged across participants and mapped onto the cortical surface. To determine which resting-state anti-correlation map was closer to the task-based map, we calculated the averaged Dice coefficient across the whole brain vertices for each participant, and then compared the Dice coefficient using a paired *t*-test. The schematic diagram of this analysis is shown in Fig. S1D. We additionally calculated the Dice overlap between the Rest-no GSR and Rest-GSR conditions, as well as the spatial correlation of their anti-correlation degrees.

**2.3.3. Effect of motion on anti-correlations:** Because the data processed without GSR likely contains more noise, we sought to determine whether motion is related to the detection of anti-correlations, particularly in the no-GSR condition. We performed Pearson correlations between motion and degree of anti-correlations in the Rest-no GSR and Rest-GSR conditions. Then, we divided the HCP participants into three equal groups according to their motion: low, medium, and high, and considered the lower- and higher-motion groups. Within each group, we performed Pearson correlations between motion and normalized degree of anti-correlations, and compared each condition with the Task condition to determine similarity in anti-correlation profiles, using the Dice coefficient.

**2.3.4. Relationship between anti-correlations and rTMS clinical efficacy:** rTMS is used clinically for the treatment of depression. rTMS treatment targeting the left DLPFC can affect remote brain regions that are connected to the DLPFC such as the sgACC (Fox et al., 2012b; Paus et al., 1997; Siebner et al., 2009) and this remote influence may mediate its antidepressant effect (Fox et al., 2012a, 2013; Weigand et al., 2018). Here, we re-analyzed the data from a previous report (Weigand et al., 2018) in which it was shown that the

strength of resting-state negative functional connectivity between rTMS DLPFC sites and sgACC, as measured in healthy participants from the Brain Genomics Superstruct Project dataset (Buckner et al., 2014), is related to the therapeutic efficacy of rTMS in a sample of 25 patients with depression. The new contribution we bring here is the calculation of normative, population-based connectivity between the rTMS sites and the sgACC using all 47 task contrasts of the HCP dataset.

BDI scores were recorded for the 25 patients with treatment-resistant major depressive disorder. Percent change in BDI scores from pre- to post-rTMS treatment were calculated. To quantify the relationship between anti-correlations and rTMS clinical efficacy, we calculated the population-level correlation coefficients between the sgACC and each of the left DLPFC seed using resting-state fMRI data as well as task data from the HCP cohort. For the resting-state data, we calculated functional connectivity between each of the 25 left DLPFC sites and sgACC for each participant, then averaged the functional connectivity across HCP participants. For the task data, we calculated co-activations between each of the left DLPFC seeds and the sgACC based on the concatenated 47 task contrasts (Table 1), then averaged co-activations across all HCP participants. Then, one-tailed Spearman correlations were calculated between the population-level DLPFC-sgACC coactivation-based connectivity and percent change in BDI scores. We repeated the same analysis using baseline BDI scores as a covariate, since more severely depressed patients have more room for symptom improvement, which is a factor that may bias the results. Results were deemed statistically significant if $p$ values were below 0.05.

### 2.4. Control analyses

Our in-house resting-state preprocessing pipeline includes motion regression, and therefore applying it to ICA-FIX processed HCP data means that two motion regressions were performed on the resting-state data. To assess whether the second motion regression impacted the data, we generated functional connectivity maps in three randomly chosen HCP participants, using the PCC as a seed, and compared the maps derived from data processed with one or two motion regressions. This was done using GSR- and non-GSR-processed data. We calculated the similarity in functional connectivity maps using Pearson correlations.

Next, the WM (19 contrasts) and Motor (13 contrasts) task contrasts made up 68% of the 47 contrasts we used in our initial analysis. There is a possibility that the pattern of task anti-correlations we detected was dominated by the ani-correlations exhibited within these two tasks. To verify whether this was the case or not, we replicated the anti-correlation analysis, this time removing the 32 contrasts from the WM and Motor tasks and only including the 15 remaining contrasts (Language, Gambling, Relational, Social, and Emotion contrasts; Table 1).

Third, as the DN exhibited the greatest degree of anti-correlations (see Fig. 3 B), we performed another control analysis to investigate whether the pattern of anti-correlations we detected was driven by connections in the DN. We recalculated the degree of anti-correlations based on connections not included in the DN.

### 2.5. Visualization

For the purpose of visualization, all imaging results were visualized using the Connectome Workbench display tool provided by the HCP (https://www.humanconnectome.org/).

### 2.6. Data and code availability

The dataset HCP were publicly available through the NIH Human Connectome Project (https://www.humanconnectome.org/). MATLAB codes that support the findings of this study are available from http://nmr.mgh.harvard.edu/bid/DownLoad.html.

## 3. Results

### 3.1. Individual seeds show anti-correlations with other brain regions during task performance and during rest

For heuristic purposes, we plotted the 47 beta values of the PCC, MTG (from DN), and FEF (from DAN) seeds to visually check for activity with correlated and opposite fluctuations during task performance at the level of a single HCP individual chosen at random (Fig. 1 A). The DN and DAN are usually found to be anti-correlated at rest (Esposito et al., 2018; Fox et al., 2005; Fransson, 2005; Raichle, 2015), therefore we expected that the concatenated beta values for these two sets of seeds (PCC vs. FEF) would show opposite fluctuations in task fMRI activation, while the two DN seeds (PCC vs. MTG), because they are within the same network, would show similar fluctuations in task fMRI activation. This is evident in Fig. 1. The FEF's fMRI activation generally runs opposite to the PCC's ($r = -0.67$) while the MTG's is positively correlated with the PCC's ($r = 0.73$). The PCC-based co-activation map (Fig. 1 B) reveals both positive correlations and anti-correlations with other vertices on the cortical surface, whether at the individual level or at the group level, whereby the PCC exhibits positive correlations with the MTG and anti-correlations with the FEF (as seen in the concatenated task contrasts). Therefore, at first glance, the task coactivation-based results generally match what is typically observed in the resting-state literature.

Next, we set out to investigate anti-correlations in three conditions reflecting different brain states and preprocessing techniques: co-activation patterns during task fMRI (Task), resting-state fMRI BOLD data with GSR applied during preprocessing (Rest-GSR), and resting-state fMRI BOLD data without GSR (Rest-no GSR). We measured whole-brain correlations in the HCP sample using the two sets of seeds from the DN (PCC, mPFC, pIPL, and MTG) and DAN (area MT+, SPL, FEF, and IFJ). We found that anti-correlations are present for every seed in all three conditions (Fig. 2 A), indicating that an antagonistic relation can be observed between networks across various cognitive states. Different seeds of the DN show variable anti-correlations with the DAN, demonstrating variability in the organization of functional subsystems of the DN and DAN. The resting-state functional connectivity maps, preprocessed without GSR, likewise demonstrate the presence of anti-correlations. As expected, anti-correlations are enhanced in the GSR-preprocessed resting-state condition. On the surface, anti-correlations appear most widely distributed and strongest in the Rest-GSR condition, more sparse and weaker in the Rest-no GSR condition, and lie somewhere in between in the Task condition. Overall, the PCC, mPFC, pIPL, and MTG are generally anti-correlated with the DAN regions (MT+, SPL, FEF, and IFJ) and their correlations maps

resemble inverted images of one another (for example, yellow regions in the PCC maps are blue in the MT+ maps, and vice versa). Importantly, the spatial distribution of the anti-correlations observed across aggregated task activations is more similar to that observed during resting-state with GSR than during resting-state without GSR (Fig. 2 B, paired *t*-test, $p<0.0001$ for all seeds except for the SPL seed).

To assess whether the second motion regression in our complete resting-state preprocessing pipeline impacted functional connectivity, we calculated the functional connectivity of the PCC in three randomly chosen HCP participants, and generated functional connectivity maps based on data preprocessed with and without the second motion regression, using the GSR as well as the non-GSR pipelines. Fig. S2 shows that the functional connectivity maps corresponding to data with one or two motion regressions are extremely similar, in both the GSR- and non-GSR-processed data, for all three participants. In fact, the spatial correlation was $r = 0.999$ across participants, for both the GSR and non-GSR data. Thus, the second motion regression did not impact the data.

### 3.2. The default network exhibits robust anti-correlations with many regions across various tasks and during rest

Our second aim was to investigate the degree to which each vertex is anti-correlated with all other vertices on the cortical surface. We calculated, for each vertex, the number of negative correlations they exhibited and plotted these on cortical surface maps. Fig. 3 A shows the absolute degree of anti-correlations to showcase the difference between all three conditions, while Fig. 3 B shows the normalized degree, to facilitate the visualization of the distribution of anti-correlations across the cortical surface. All vertices demonstrate anti-correlations with other brain regions, suggesting that anti-correlations are a ubiquitous feature of brain activity (Fig. 3 A). DN areas, including the dorsolateral prefrontal cortex, medial prefrontal cortex, lateral temporal cortex, lateral parietal cortex, and the posterior midline (precuneus and PCC), as well as limbic network regions, like the ventromedial prefrontal cortex and medial temporal lobe, exhibit the greatest degree of anti-correlations (Fig. 3 B). This is true for the anti-correlations observed across tasks, as well as during rest (Rest-no GSR, and Rest-GSR conditions).

Because the WM and Motor task contrasts made up the majority of the contrasts (32/47), as control analysis, we investigated the degree of anti-correlations in the remaining 15 contrasts. This was done to make sure that the pattern of anti-correlations we detected was not driven by the co-activations in the WM and Motor tasks. Fig. S3 shows the degree of anti-correlations using these 15 task contrasts. The distribution of anti-correlations is very similar to that detected using all 47 contrasts ($r = 0.78$), indicating that the WM and Motor tasks did not exert a disproportionate effect on the results. The anti-correlation distribution therefore appears to be robust.

Many of the anti-correlations we detected are located in the DN. To verify that the distribution of anti-correlations was not driven by seeds in the DN, we recalculated the degree of anti-correlations solely based on seeds outside of the DN (Fig. S4A). The distributions, with and without DN seeds, were found to be highly similar ($r = 0.76$; Fig.

S4B), indicating that the DN seeds did not drive the finding. Thus, seeds inside and outside of the DN show pronounced anti-correlations with DN regions.

Following this, we compared the anti-correlation profiles observed across the aggregated tasks to those observed in i) the Rest-no GSR condition, and; ii) the Rest-GSR condition, by calculating the Dice coefficient of anti-correlations for each seed vertex, averaged across participants (Fig. 3 C, left). Interestingly, regions with greater degrees of anti-correlations (Fig. 3 B) display greater similarity between conditions (Fig. 3 C, left). The Dice coefficients overall are significantly greater for the Rest-GSR (mean Dice value = 0.433) condition than for the Rest-no GSR (mean Dice value = 0.370) condition (paired *t*-test: $t(679) = 36$, $p < 0.0001$; Fig. 3 C, right), indicating that rs-fcMRI data processed with GSR is a better predictor of task-induced modulation than rs-fcMRI processed without GSR. We also directly compared the distribution of anti-correlation degrees between the Rest-no GSR and Rest-GSR conditions, and found them to be highly similar (spatial correlation: $r = 0.58$; see Fig. S5 for Dice coefficient map).

Because the data processed without GSR likely contained more noise in the signal, we performed control analyses to investigate the relation between anti-correlations and head motion. As expected, we found a significant relationship in the Rest-no GSR condition, whereby greater motion is related to a smaller normalized degree of anti-correlations ($r = -0.13$, $p < 0.001$), while there is no such relationship in the Rest-GSR condition ($r = -0.025$, $p = 0.52$) (Fig. 4 A). We then considered two subgroups of participants: one with lower motion ($N = 220$; average motion: 0.058 ± 0.006 mm) and one with higher motion ($N = 220$; average motion: 0.101 ± 0.012) and again investigated the motion effect on anti-correlation detection. In the low-motion group, although the impact of motion on anti-correlations is insignificant for the Rest-no GSR condition ($r = 0.054$, $p = 0.426$), anti-correlation profiles remain more similar between Task and Rest-GSR conditions than between Task and Rest-no GSR conditions (paired *t*-test: $t(219) = 19$, $p < 0.0001$) (Fig. 4 B, left). In the higher-motion group, again there is no significant relationship between anti-correlation and head motion for the Rest-no GSR ($r = -0.006$, $p = 0.926$) condition (Fig. 4 B, right) and the Task condition also exhibits anti-correlation profiles more similar to Rest-GSR than to Rest-no GSR (paired *t*-test: $t(219) = 22$, $p < 0.0001$). Thus, these results indicate that even when there is limited head motion, anti-correlation profiles found during task-fMRI are still more similar to those found in resting-state data processed with than without GSR.

### 3.3. Anti-correlations between networks can lead to meaningful clinical biomarkers

Using the rTMS dataset, we first replicated the findings in (Weigand et al., 2018) using resting-state fMRI data and confirmed that the negative functional connectivity between the rTMS sites and the sgACC tracked with treatment response, measured as percent change in BDI scores (Rest-GSR: $r = -0.42$, $p = 0.019$). Next, we investigated the same relationship, this time using task-based co-activations to estimate rTMS site-sgACC anti-correlations, which has never before been done using this dataset. Using correlations derived from the 47 task-based beta maps, we found that correlations between patients' rTMS sites and the sgACC significantly tracked with treatment efficacy ($r = -0.37$, $p = 0.036$; Fig. 5), indicating that the stronger the DLPFC-sgACC anti-correlation, the better the rTMS clinical efficacy.

As more severely depressed patients have more room for symptom improvement, we conducted the same analysis while covarying with baseline BDI scores to mitigate it as a confounding factor. The relationship between rTMS sites-sgACC co-activation and BDI improvement remained significant ($r = -0.44$, $p = 0.016$). These results from independent imaging modalities suggest that anti-correlations between networks, regardless of brain state, can lead to meaningful clinical biomarkers.

## 4. Discussion

In this study, we examined whether anti-correlated networks are a meaningful principle of functional brain organization. We did this by investigating correlations based on co-activation patterns across a variety of tasks. Such analysis is free of the mathematical mandate that is inherent to GSR preprocessing in resting-state fMRI analysis. Our results revealed the presence of non-artifactual anti-correlations in brain activity during task performance. Moreover, anti-correlations seen in resting-state data processed with GSR are a better predictor of how brain activity fluctuates across tasks compared to resting-state data processed without GSR. We then retrospectively analyzed data from a previous report (Weigand et al., 2018) and found that task-based anti-correlations track with rTMS treatment efficacy in a cohort of patients with medication-resistant depression. Taken together, our results point to a neurobiological role for anti-correlations in human functional brain organization.

### 4.1. Anti-correlations are a fundamental principle of brain functional organization

In the current study, we investigated anti-correlations in task fMRI and resting-state fMRI from the same cohort of healthy participants. Anti-correlated activations across various tasks show similar spatial patterns as the anti-correlated functional connectivity commonly observed in resting-state data. Using several landmark seeds from the DN and DAN, anti-correlations were found across all seeds at the group level, regardless of brain states (task or rest) or preprocessing techniques used (GSR or no-GSR). Critically, the absence of a mathematical mandate for anti-correlations in task-based activity provides compelling evidence that anti-correlations among brain regions are a real phenomenon and non-artifactual.

Antagonistic relationships between brain networks, either during resting-state (i.e., anti-correlated BOLD signals) or in a particular task, have been widely recognized in the past (Barber et al., 2013; Chai et al., 2012; Esposito et al., 2018; Fransson, 2005; Hampson et al., 2010; Raichle, 2015; Spreng et al., 2016). This competing relationship between networks can be impaired in mental diseases (Sorg et al., 2007; Wang et al., 2007; Whitfield-Gabrieli et al., 2009) and may correlate with different cognitive abilities (Kelly et al., 2008; Thompson et al., 2013). Our observations in the current study add to this previous evidence and suggest that the human brain is organized into temporally opposing networks that may go beyond the competition between the DN and DAN.

Although a common observation in the imaging literature, the competing relationship between networks has not been systematically investigated in the past for a few technical reasons. First, the magnitude of negative correlations observed at rest, while significant, is

often considerably weaker and less spatially coherent than regions with positive correlations. Second, the inclusion of GSR in data processing makes it harder to interpret the observed negative correlations. Third, in task fMRI, the activated and deactivated areas are dependent on the task design and the opposing patterns may not easily repeat themselves in a different task. The present study overcomes these technical obstacles to some extent by examining brain activations across multiple tasks, and reveals robust opposing relationships between networks. The competition between brain networks may be the large-scale manifestation of balancing functional specialization (Passingham et al., 2002; Zeki, 1978) with functional integration (Bressler, 1995; Friston, 2002; McIntosh, 2000; Sporns, 2013; Tononi et al., 1998; Varela et al., 2001) – interacting and opposing attributes that are necessary for normal brain function.

### 4.2. The default network displays robust negative correlations with other brain regions

Based on task-induced activity, we found that all vertices on the brain surface exhibit anti-correlations with other brain regions, suggesting that anti-correlations are a ubiquitous feature of brain activity (Fig. 3). Importantly, regions belonging to the DN and the limbic networks exhibit a particularly high degree of anti-correlations (Fig. 3 A and B). This is true even when discounting seed vertices from within the DN (Fig. S4). Although the DN was initially thought to become deactivated during attention-demanding tasks as it consistently demonstrated increased activity during rest relative to task conditions (hence the name default network) (Raichle et al., 2001), it should be noted that DN activity appears to actually have meaningful fluctuations across different tasks. In a recent study, Chen et al. (2018) showed that regions generally regarded as being “task-negative” (e.g., DN regions, although they are active during certain types of tasks, such as memory tasks) are active much of the time (~46%) during task performance and that the reverse is true as well—that is, supposedly “task-positive” regions are active during resting-state (~39% of the time). While the majority of task performance is spent in a “task-positive” state, the fact that a large portion of the time is also spent in a state akin to rest, mind wandering, or remembrance, and vice versa, suggests that there are constant shifts or a cycling between supposed “task-positive” networks and the DN, whether in a resting state or in a task processing state, further antiquating the use of the terms “task-positive” and “task-negative”. The significant involvement of the DN in this cycling of brain states may also explain the DN’s role as a “hub” in brain functional connectivity (Buckner et al., 2009). Taken together, while the antagonistic interactions are not limited to specific brain networks, cycling between various networks and the DN, as reflected by anti-correlations, appears to be one of the most prominent patterns in brain network dynamics.

### 4.3. Resting-state data processed with GSR is a better predictor of task-induced modulation than data processed without GSR

Whether GSR should be included in resting-state fMRI data processing has been widely debated in the past decade and the primary concern is that GSR would bias functional connectivity towards negative correlations. In the present study, a particularly interesting observation is that, at the whole brain level, the anti-correlation profiles observed in tasks is more similar to that of GSR-preprocessed resting-state fMRI than to non-GSR preprocessed resting-state fMRI (Fig. 3 C), even when the data are not obviously affected by head motion

(Fig. 4). While our goal is not to advise for or against the use of GSR, this observation suggests that, although GSR exaggerates anti-correlations, it is helpful in revealing important characteristics of functional connectivity that may go undetected when GSR is not applied. The difference in overall similarity is small (Fig. 3 C, right), and the GSR and no-GSR anti-correlation distributions are highly similar, as evidenced by the Dice coefficient map showing high overlap between the two conditions (Fig. S5). The variability in similarity across the cortical surface (Fig. 3 C, left), however, implies that some regions are likely more greatly affected than others. Bypassing GSR could diminish sensitivity to negative interactions, a fundamental property of brain networks that was robustly detected in activation/deactivation patterns across tasks, and could do so in a widespread manner or in a region-specific manner. While GSR has its caveats (see Introduction), recent studies demonstrate some clear advantages depending on the objective of the study. For example, Power et al. (2017b) compared various combinations of denoising strategies. They showed that GSR is the only denoising method that effectively removes global signals, including artifactual signals and, crucially, global neural activity (Power et al., 2017b; although see Aquino et al., 2020) which is proposed to be modulated mainly by respiration and/or arousal/vigilance (falling asleep is related to slower and deeper breathing (Power et al., 2017a, 2017b)). Therefore, GSR is particularly useful in studies that wish to control for global neural activity (e.g., controlling for tiredness), but should be avoided in studies in which the global neural signal is of interest, as for example in arousal or sleep studies (Power et al., 2017a). We speculate that the removal of global neural signals related to arousal or tiredness may explain why our GSR-preprocessed data reveals interactions that are more similar to those observed in task fMRI, as performing tasks inside the scanner helps keep participants awake and vigilant, while task-free fMRI is more conducive to sleep or to a relaxed state. The greater similarity could also be due to the removal of respiratory-related artifacts from the resting-state data. Although these effects were not removed from the task fMRI data, one may suppose that task fMRI contrasts would be less prone to respiratory effects as the act of contrasting two conditions may cancel out extraneous factors, although this may be subject to task design (e.g., trial length, whether conditions are interleaved, etc.).

### 4.4. Anti-correlations can lead to meaningful clinical biomarkers

In depression, the most common and efficacious neuromodulatory therapies are rTMS of the left DLPFC and deep-brain stimulation (DBS) of the sgACC, both of which have a good track record (Carpenter et al., 2012; Connolly et al., 2012; Fitzgerald et al., 2009; George et al., 2010; Lozano et al., 2012; Mayberg et al., 2005; O'Reardon et al., 2007; Schlaepfer et al., 2013; Weigand et al., 2018). Fox et al. (2014) have shown that these targets are functionally connected and demonstrate anti-correlations, leading them to propose that stimulation of these regions may act on the same disease-specific neural network. Especially relevant to the current topic, the authors showed that a number of disorders benefit from the stimulation of sites that display anti-correlations between one another (i.e. anti-correlated network nodes), where excitatory stimulation of one site or inhibitory stimulation of the other both lead to symptomatic improvement. Besides depression, stimulation of anti-correlated sites lead to therapeutic effects in Parkinson' disease, addiction, Alzheimer's disease, anorexia, gait dysfunction, and pain (see Fig. 2 in Fox et al. (2014)). Thus, anti-

correlations are meaningful in that they can help identify stimulation sites that have the potential of imparting beneficial effects in several neurologic and psychiatric disorders.

In our study, the meaningfulness of anti-correlations was further examined in a clinical cohort of 25 patients with depression. We investigated whether task-based population-level anti-correlations can predict clinical efficacy in patients who underwent rTMS. We found that task-based anti-correlations between rTMS sites and bilateral sgACC significantly predict rTMS therapeutic efficacy. Moreover, using resting-state fMRI data, we found that the DLPFC-sgACC anti-correlation is a predictor regardless of which preprocessing technique was used. While the investigation of the impact of GSR on the detection of individual differences is a new endeavor and there is evidence for (Li et al., 2019b) and against (Li et al., 2019a) the use of GSR in this context, we found associations of similar strengths between anti-correlations and individual clinical efficacy with and without GSR.

In summary, we found that anti-correlations are a ubiquitous feature of human brain networks and organization, that they are present all over cortex, regardless of brain state, and that they are biologically meaningful and may be especially relevant in clinical contexts.

### 4.5. Limitations and future directions

There are several limitations of the study that are worth mentioning. First, tasks involve biases in co-activation patterns that are related to task demands (for example, button presses in response to visual stimuli would induce a co-activation between primary visual and somatomotor areas). However, these biases were mitigated through the use of multiple tasks, therefore these confounds may not affect anti-correlations. Second, we have used a limited number of task contrasts to estimate the co-activation patterns between brain regions, and the contrasts are not strictly independent from one another. As a result, the statistical significance of the correlations and anti-correlations derived from task-activations may have been overestimated. Nevertheless, in the current study, we mainly focused on the direction of correlations (i.e., positive or negative correlations) rather than the significance of the correlations per se. Third, we analyzed task and resting-state data from the HCP in order to examine to what extent anti-correlations track with rTMS treatment response in a sample of patients with depression. While these anti-correlations were not investigated at the level of the clinical sample, the use of HCP as normative data confers the advantage of providing robust population-level observations (Weigand et al., 2018). It is important to note that the relationship between anti-correlations and clinical efficacy has been reproduced using patient resting-state fMRI data (Fox et al., 2014, 2012a). We posit that future studies using seeds identified at the individual level (Wang et al., 2015) may increase precision and the detection of more robust effects.

## Supplementary Material

Refer to Web version on PubMed Central for supplementary material.

## Acknowledgments

The authors thank Dr. Paola Galdi and Dr. Julien Dubois for sharing the Python-based data preprocessing pipeline code, as well as Dr. Ru Kong for sharing the 1483 sparse vertices in 32k fsLR space. The primary data was

provided by the Human Connectome Project, WU-Minn Consortium (Principal Investigators: David Van Essen and Kamil Ugurbil; 1U54MH091657), funded by the 16 NIH Institutes and Centers that support the NIH Blueprint for Neuroscience Research; and by the Mc-Donnell Center for Systems Neuroscience at Washington University. We thank the National Center for Protein Sciences at Peking University for assistance with MRI data processing tools.

**Funding**

This work was supported by the National Key Research and Development Program of China (2016YFC1306303), National Institutes of Health grants R01NS091604, P50MH106435 and K01MH111802, and by the National Natural Science Foundation of China grants no. 81790650, 81790652, 81522021, 81671285, 81790653, 81790654 and 81671662. L.D. is supported by a Canadian Institutes of Health Research postdoctoral fellowship, FRN: MFE-171291.

## References

Aquino KM, Fulcher BD, Parkes L, Sabaroedin K, Fornito A, 2020. Identifying and removing widespread signal deflections from fMRI data: rethinking the global signal regression problem. Neuroimage 212, 116614. [PubMed: 32084564]

Barber AD, Caffo BS, Pekar JJ, Mostofsky SH, 2013. Developmental changes in within- and between-network connectivity between late childhood and adulthood. Neuropsychologia 51, 156–167. [PubMed: 23174403]

Barch DM, Burgess GC, Harms MP, Petersen SE, Schlaggar BL, Corbetta M, Glasser MF, Curtiss S, Dixit S, Feldt C, Nolan D, Bryant E, Hartley T, Footer O, Bjork JM, Poldrack R, Smith S, Johansen-Berg H, Snyder AZ, Van Essen DC, 2013. Function in the human connectome: task-fMRI and individual differences in behavior. Neuroimage 80, 169–189. [PubMed: 23684877]

Boes AD, Prasad S, Liu H, Liu Q, Pascual-Leone A, Caviness VS Jr, Fox MD, 2015. Network localization of neurological symptoms from focal brain lesions. Brain 138, 3061–3075. [PubMed: 26264514]

Bressler SL, 1995. Large-scale cortical networks and cognition. Brain Res. Rev 20, 288–304. [PubMed: 7550362]

Buckner R, Roffman J, Smoller J, 2014. Brain genomics superstruct project (GSP). Harv. Dataverse 10.

Buckner RL, Sepulcre J, Talukdar T, Krienen FM, Liu H, Hedden T, Andrews-Hanna JR, Sperling RA, Johnson KA, 2009. Cortical hubs revealed by intrinsic functional connectivity: mapping, assessment of stability, and relation to Alzheimer's disease. J. Neurosci 29, 1860–1873. [PubMed: 19211893]

Carpenter LL, Janicak PG, Aaronson ST, Boyadjis T, Brock DG, Cook IA, Dunner DL, Lanocha K, Solvason HB, Demitrack MA, 2012. Transcranial magnetic stimulation (TMS) for major depression: a multisite, naturalistic, observational study of acute treatment outcomes in clinical practice. Depress. Anxiety 29, 587–596. [PubMed: 22689344]

Cash RF, Zalesky A, Thomson RH, Tian Y, Cocchi L, Fitzgerald PB, 2019. Subgenual functional connectivity predicts antidepressant treatment response to transcranial magnetic stimulation: independent validation and evaluation of personalization. Biol. Psychiatry

Chai XJ, Castanon AN, Ongur D, Whitfield-Gabrieli S, 2012. Anticorrelations in resting state networks without global signal regression. Neuroimage 59, 1420–1428. [PubMed: 21889994]

Chang C, Leopold DA, Schölvinck ML, Mandelkow H, Picchioni D, Liu X, Ye FQ, Turchi JN, Duyn JH, 2016. Tracking brain arousal fluctuations with fMRI. Proc. Natl. Acad. Sci 113, 4518–4523. [PubMed: 27051064]

Chen RH, Ito T, Kulkarni KR, Cole MW, 2018. The human brain traverses a common activation-pattern state space across task and rest. Brain Connect. 8, 429–443. [PubMed: 29999413]

Ciric R, Wolf DH, Power JD, Roalf DR, Baum GL, Ruparel K, Shinohara RT, Elliott MA, Eickhoff SB, Davatzikos C, Gur RC, Gur RE, Bassett DS, Satterthwaite TD, 2017. Benchmarking of participant-level confound regression strategies for the control of motion artifact in studies of functional connectivity. Neuroimage 154, 174–187. [PubMed: 28302591]

Connolly KR, Helmer A, Cristancho MA, Cristancho P, O'Reardon JP, 2012. Effectiveness of transcranial magnetic stimulation in clinical practice post-FDA approval in the United States:

results observed with the first 100 consecutive cases of depression at an academic medical center. J. Clin. Psychiatry 73, e567–e573. [PubMed: 22579164]

Dubois J, Galdi P, Han Y, Paul LK, Adolphs R, 2018. Resting-state functional brain connectivity best predicts the personality dimension of openness to experience. Personal. Neurosci 1, e6. [PubMed: 30225394]

Esposito R, Cieri F, Chiacchiaretta P, Cera N, Lauriola M, Di Giannantonio M, Tartaro A, Ferretti A, 2018. Modifications in resting state functional anticorrelation between default mode network and dorsal attention network: comparison among young adults, healthy elders and mild cognitive impairment patients. Brain Imaging Behav. 12, 127–141. [PubMed: 28176262]

Fitzgerald PB, Hoy K, McQueen S, Maller JJ, Herring S, Segrave R, Bailey M, Been G, Kulkarni J, Daskalakis ZJ, 2009. A randomized trial of rTMS targeted with MRI based neuro-navigation in treatment-resistant depression. Neuropsychopharmacology 34, 1255. [PubMed: 19145228]

Fox MD, 2018. Mapping symptoms to brain networks with the human connectome. N. Engl. J. Med 379, 2237–2245. [PubMed: 30575457]

Fox MD, Buckner RL, Liu H, Chakravarty MM, Lozano AM, Pascual-Leone A, 2014. Resting-state networks link invasive and noninvasive brain stimulation across diverse psychiatric and neurological diseases. Proc. Natl. Acad. Sci 111, E4367–E4375. [PubMed: 25267639]

Fox MD, Buckner RL, White MP, Greicius MD, Pascual-Leone A, 2012a. Efficacy of transcranial magnetic stimulation targets for depression is related to intrinsic functional connectivity with the subgenual cingulate. Biol. Psychiatry 72, 595–603. [PubMed: 22658708]

Fox MD, Halko MA, Eldaief MC, Pascual-Leone A, 2012b. Measuring and manipulating brain connectivity with resting state functional connectivity magnetic resonance imaging (fcMRI) and transcranial magnetic stimulation (TMS). Neuroimage 62, 2232–2243. [PubMed: 22465297]

Fox MD, Liu H, Pascual-Leone A, 2013. Identification of reproducible individualized targets for treatment of depression with TMS based on intrinsic connectivity. Neuroimage 66, 151–160. [PubMed: 23142067]

Fox MD, Snyder AZ, Vincent JL, Corbetta M, Van Essen DC, Raichle ME, 2005. The human brain is intrinsically organized into dynamic, anticorrelated functional networks. Proc. Natl. Acad. Sci. U.S.A 102, 9673–9678. [PubMed: 15976020]

Fox MD, Zhang D, Snyder AZ, Raichle ME, 2009. The global signal and observed anticorrelated resting state brain networks. J. Neurophysiol 101, 3270–3283. [PubMed: 19339462]

Fransson P, 2005. Spontaneous low-frequency BOLD signal fluctuations: an fMRI investigation of the resting-state default mode of brain function hypothesis. Hum. Brain Mapp 26, 15–29. [PubMed: 15852468]

Friston K, 2002. ACRH ReportsFunctional integration and inference in the brain. Prog. Neurobiol 68, 113–143. [PubMed: 12450490]

George MS, Lisanby SH, Avery D, McDonald WM, Durkalski V, Pavlicova M, Anderson B, Nahas Z, Bulow P, Zarkowski P, 2010. Daily left prefrontal transcranial magnetic stimulation therapy for major depressive disorder: a sham-controlled randomized trial. Arch. Gen. Psychiatry 67, 507–516. [PubMed: 20439832]

Glasser MF, Coalson TS, Robinson EC, Hacker CD, Harwell J, Yacoub E, Ugurbil K, Andersson J, Beckmann CF, Jenkinson M, 2016. A multi-modal parcellation of human cerebral cortex. Nature 536, 171. [PubMed: 27437579]

Hampson M, Driesen N, Roth JK, Gore JC, Constable RT, 2010. Functional connectivity between task-positive and task-negative brain areas and its relation to working memory performance. Magn. Reson. Imaging 28, 1051–1057. [PubMed: 20409665]

Kelly AM, Uddin LQ, Biswal BB, Castellanos FX, Milham MP, 2008. Competition between functional brain networks mediates behavioral variability. Neuroimage 39, 527–537. [PubMed: 17919929]

Kong R, Li J, Orban C, Sabuncu MR, Liu H, Schaefer A, Sun N, Zuo XN, Holmes AJ, Eickhoff SB, Yeo BTT, 2019. Spatial topography of individual-specific cortical networks predicts human cognition, personality, and emotion. Cereb. Cortex 29, 2533–2551. [PubMed: 29878084]

Li J, Bolt T, Bzdok D, Nomi JS, Yeo BTT, Spreng RN, Uddin LQ, 2019a. Topography and behavioral relevance of the global signal in the human brain. Sci. Rep 9, 14286. [PubMed: 31582792]

Li J, Kong R, Liégeois R, Orban C, Tan Y, Sun N, Holmes AJ, Sabuncu MR, Ge T, Yeo BTT, 2019b. Global signal regression strengthens association between resting-state functional connectivity and behavior. Neuroimage 196, 126–141. [PubMed: 30974241]

Liu T, Nalci A, Falahpour M, 2017. The global signal in fMRI: nuisance or Information? Neuroimage 150.

Liu X, de Zwart JA, Schölvinck ML, Chang C, Ye FQ, Leopold DA, Duyn JH, 2018. Subcortical evidence for a contribution of arousal to fMRI studies of brain activity. Nat. Commun 9, 395. [PubMed: 29374172]

Lozano AM, Giacobbe P, Hamani C, Rizvi SJ, Kennedy SH, Kolivakis TT, Debonnel G, Sadikot AF, Lam RW, Howard AK, 2012. A multicenter pilot study of subcallosal cingulate area deep brain stimulation for treatment-resistant depression. J. Neurosurg 116, 315–322. [PubMed: 22098195]

Mayberg HS, Lozano AM, Voon V, McNeely HE, Seminowicz D, Hamani C, Schwalb JM, Kennedy SH, 2005. Deep brain stimulation for treatment-resistant depression. Neuron 45, 651–660. [PubMed: 15748841]

McIntosh AR, 2000. Towards a network theory of cognition. Neural Netw. 13, 861–870. [PubMed: 11156197]

Murphy K, Birn RM, Handwerker DA, Jones TB, Bandettini PA, 2009. The impact of global signal regression on resting state correlations: are anti-correlated networks introduced? Neuroimage 44, 893–905. [PubMed: 18976716]

Murphy K, Fox MD, 2017. Towards a consensus regarding global signal regression for resting state functional connectivity MRI. Neuroimage 154, 169–173. [PubMed: 27888059]

O'Reardon JP, Solvason HB, Janicak PG, Sampson S, Isenberg KE, Nahas Z, McDonald WM, Avery D, Fitzgerald PB, Loo C, 2007. Efficacy and safety of transcranial magnetic stimulation in the acute treatment of major depression: a multisite randomized controlled trial. Biol. Psychiatry 62, 1208–1216. [PubMed: 17573044]

Orban C, Kong R, Li J, Chee MWL, Yeo BTT, 2020. Time of day is associated with paradoxical reductions in global signal fluctuation and functional connectivity. PLoS Biol. 18, e3000602. [PubMed: 32069275]

Parkes L, Fulcher B, Yücel M, Fornito A, 2018. An evaluation of the efficacy, reliability, and sensitivity of motion correction strategies for resting-state functional MRI. Neuroimage 171, 415–436. [PubMed: 29278773]

Passingham RE, Stephan KE, Kötter R, 2002. The anatomical basis of functional localization in the cortex. Nat. Rev. Neurosci 3, 606–616. [PubMed: 12154362]

Paus T, Jech R, Thompson CJ, Comeau R, Peters T, Evans AC, 1997. Transcranial magnetic stimulation during positron emission tomography: a new method for studying connectivity of the human cerebral cortex. J. Neurosci 17, 3178–3184. [PubMed: 9096152]

Power JD, Laumann TO, Plitt M, Martin A, Petersen SE, 2017a. On global fMRI signals and simulations. Trends Cogn. Sci. Regul. Ed 21, 911–913.

Power JD, Plitt M, Laumann TO, Martin A, 2017b. Sources and implications of whole-brain fMRI signals in humans. Neuroimage 146, 609–625. [PubMed: 27751941]

Raichle ME, 2015. The brain's default mode network. Annu. Rev. Neurosci 38, 433–447. [PubMed: 25938726]

Raichle ME, MacLeod AM, Snyder AZ, Powers WJ, Gusnard DA, Shulman GL, 2001. A default mode of brain function. Proc. Natl. Acad. Sci 98, 676–682. [PubMed: 11209064]

Schölvinck ML, Maier A, Ye FQ, Duyn JH, Leopold DA, 2010. Neural basis of global resting-state fMRI activity. Proc. Natl. Acad. Sci. U.S.A 107, 10238–10243. [PubMed: 20439733]

Schlaepfer TE, Bewernick BH, Kayser S, Mädler B, Coenen VA, 2013. Rapid effects of deep brain stimulation for treatment-resistant major depression. Biol. Psychiatry 73, 1204–1212. [PubMed: 23562618]

Shen X, Finn ES, Scheinost D, Rosenberg MD, Chun MM, Papademetris X, Constable RT, 2017. Using connectome-based predictive modeling to predict individual behavior from brain connectivity. Nat. Protoc 12, 506. [PubMed: 28182017]

Siebner HR, Bergmann TO, Bestmann S, Massimini M, Johansen-Berg H, Mochizuki H, Bohning DE, Boorman ED, Groppa S, Miniussi C, 2009. Consensus paper: combining transcranial stimulation with neuroimaging. Brain Stimul. 2, 58–80. [PubMed: 20633405]

Siegel JS, Mitra A, Laumann TO, Seitzman BA, Raichle M, Corbetta M, Snyder AZ, 2017. Data quality influences observed links between functional connectivity and behavior. Cereb. Cortex 27, 4492–4502. [PubMed: 27550863]

Smith SM, Beckmann CF, Andersson J, Auerbach EJ, Bijsterbosch J, Douaud G, Duff E, Feinberg DA, Griffanti L, Harms MP, 2013. Resting-state fMRI in the human connectome project. Neuroimage 80, 144–168. [PubMed: 23702415]

Sorg C, Riedl V, Mühlau M, Calhoun VD, Eichele T, Läer L, Drzezga A, Förstl H, Kurz A, Zimmer C, Wohlschläger AM, 2007. Selective changes of resting-state networks in individuals at risk for Alzheimer's disease. Proc. Natl. Acad. Sci. U.S.A 104, 18760–18765. [PubMed: 18003904]

Sporns O, 2013. Network attributes for segregation and integration in the human brain. Curr. Opin. Neurobiol 23, 162–171. [PubMed: 23294553]

Spreng RN, Stevens WD, Viviano JD, Schacter DL, 2016. Attenuated anticorrelation between the default and dorsal attention networks with aging: evidence from task and rest. Neurobiol. Aging 45, 149–160. [PubMed: 27459935]

Thompson GJ, Magnuson ME, Merritt MD, Schwarb H, Pan WJ, McKinley A, Tripp LD, Schumacher EH, Keilholz SD, 2013. Short-time windows of correlation between large-scale functional brain networks predict vigilance intraindividually and interindividually. Hum. Brain Mapp 34, 3280–3298. [PubMed: 22736565]

Thompson GJ, Riedl V, Grimmer T, Drzezga A, Herman P, Hyder F, 2016. The whole-brain "global" signal from resting state fMRI as a potential biomarker of quantitative state changes in glucose metabolism. Brain Connect. 6, 435–447. [PubMed: 27029438]

Tononi G, Edelman GM, Sporns O, 1998. Complexity and coherency: integrating information in the brain. Trends Cogn. Sci. Regul. Ed 2, 474–484.

Turchi J, Chang C, Ye FQ, Russ BE, Yu DK, Cortes CR, Monosov IE, Duyn JH, Leopold DA, 2018. The basal forebrain regulates global resting-state fMRI fluctuations. Neuron 97, 940–952. [PubMed: 29398365]

Van Essen DC, Smith SM, Barch DM, Behrens TE, Yacoub E, Ugurbil K, Consortium W-MH, 2013. The WU-Minn human connectome project: an overview. Neuroimage 80, 62–79. [PubMed: 23684880]

Van Essen DC, Ugurbil K, Auerbach E, Barch D, Behrens T, Bucholz R, Chang A, Chen L, Corbetta M, Curtiss SW, 2012. The human connectome project: a data acquisition perspective. Neuroimage 62, 2222–2231. [PubMed: 22366334]

Varela F, Lachaux JP, Rodriguez E, Martinerie J, 2001. The brainweb: phase synchronization and large-scale integration. Nat. Rev. Neurosci 2, 229–239. [PubMed: 11283746]

Wang D, Buckner RL, Fox MD, Holt DJ, Holmes AJ, Stoecklein S, Langs G, Pan R, Qian T, Li K, 2015. Parcellating cortical functional networks in individuals. Nat. Neurosci 18, 1853. [PubMed: 26551545]

Wang K, Liang M, Wang L, Tian L, Zhang X, Li K, Jiang T, 2007. Altered functional connectivity in early Alzheimer's disease: a resting-state fMRI study. Hum. Brain Mapp 28, 967–978. [PubMed: 17133390]

Weigand A, Horn A, Caballero R, Cooke D, Stern AP, Taylor SF, Press D, Pascual-Leone A, Fox MD, 2018. Prospective validation that subgenual connectivity predicts antidepressant efficacy of transcranial magnetic stimulation sites. Biol. Psychiatry 84, 28–37. [PubMed: 29274805]

Weissenbacher A, Kasess C, Gerstl F, Lanzenberger R, Moser E, Windischberger C, 2009. Correlations and anticorrelations in resting-state functional connectivity MRI: a quantitative comparison of preprocessing strategies. Neuroimage 47, 1408–1416. [PubMed: 19442749]

Whitfield-Gabrieli S, Thermenos HW, Milanovic S, Tsuang MT, Faraone SV, Mc-Carley RW, Shenton ME, Green AI, Nieto-Castanon A, LaViolette P, Wojcik J, Gabrieli JDE, Seidman LJ, 2009. Hyperactivity and hyperconnectivity of the default network in schizophrenia and in first-degree relatives of persons with schizophrenia. Proc. Natl. Acad. Sci 106, 1279–1284. [PubMed: 19164577]

Wong CW, Olafsson V, Tal O, Liu TT, 2013. The amplitude of the resting-state fMRI global signal is related to EEG vigilance measures. Neuroimage 83, 983–990. [PubMed: 23899724]

Woolrich MW, Ripley BD, Brady M, Smith SM, 2001. Temporal autocorrelation in univariate linear modeling of FMRI data. Neuroimage 14, 1370–1386. [PubMed: 11707093]

Wu J, Ngo GH, Greve D, Li J, He T, Fischl B, Eickhoff SB, Yeo BT, 2018. Accurate nonlinear mapping between MNI volumetric and FreeSurfer surface coordinate systems. Hum. Brain Mapp 39, 3793–3808. [PubMed: 29770530]

Yan C−G, Cheung B, Kelly C, Colcombe S, Craddock RC, Di Martino A, Li Q, Zuo X−N, Castellanos FX, Milham MP, 2013. A comprehensive assessment of regional variation in the impact of head micromovements on functional connectomics. Neuroimage 76, 183–201. [PubMed: 23499792]

Yeo T, Krienen FM, Sepulcre J, Sabuncu MR, Lashkari D, Hollinshead M, Roffman JL, Smoller JW, Zöllei L, Polimeni JR, Fischl B, Liu H, Buckner RL, 2011. The organization of the human cerebral cortex estimated by intrinsic functional connectivity. J. Neurophysiol 106, 1125–1165. [PubMed: 21653723]

Zaborszky L, Csordas A, Mosca K, Kim J, Gielow MR, Vadasz C, Nadasdy Z, 2015. Neurons in the basal forebrain project to the cortex in a complex topographic organization that reflects corticocortical connectivity patterns: an experimental study based on retrograde tracing and 3D reconstruction. Cereb. Cortex 25, 118–137. [PubMed: 23964066]

Zarahn E, Aguirre G, DEsposito M, 1997. Empirical analyses of BOLD fMRI statistics. 1. In: Spacially Unsmoothed Data Collected Under Null-Hypothesis Conditions (Vol 5, pp. 179. Academic Press Inc JNL, San Diego, CA, pp. 71–72.

Zeki SM, 1978. Functional specialisation in the visual cortex of the rhesus monkey. Nature 274, 423–428. [PubMed: 97565]

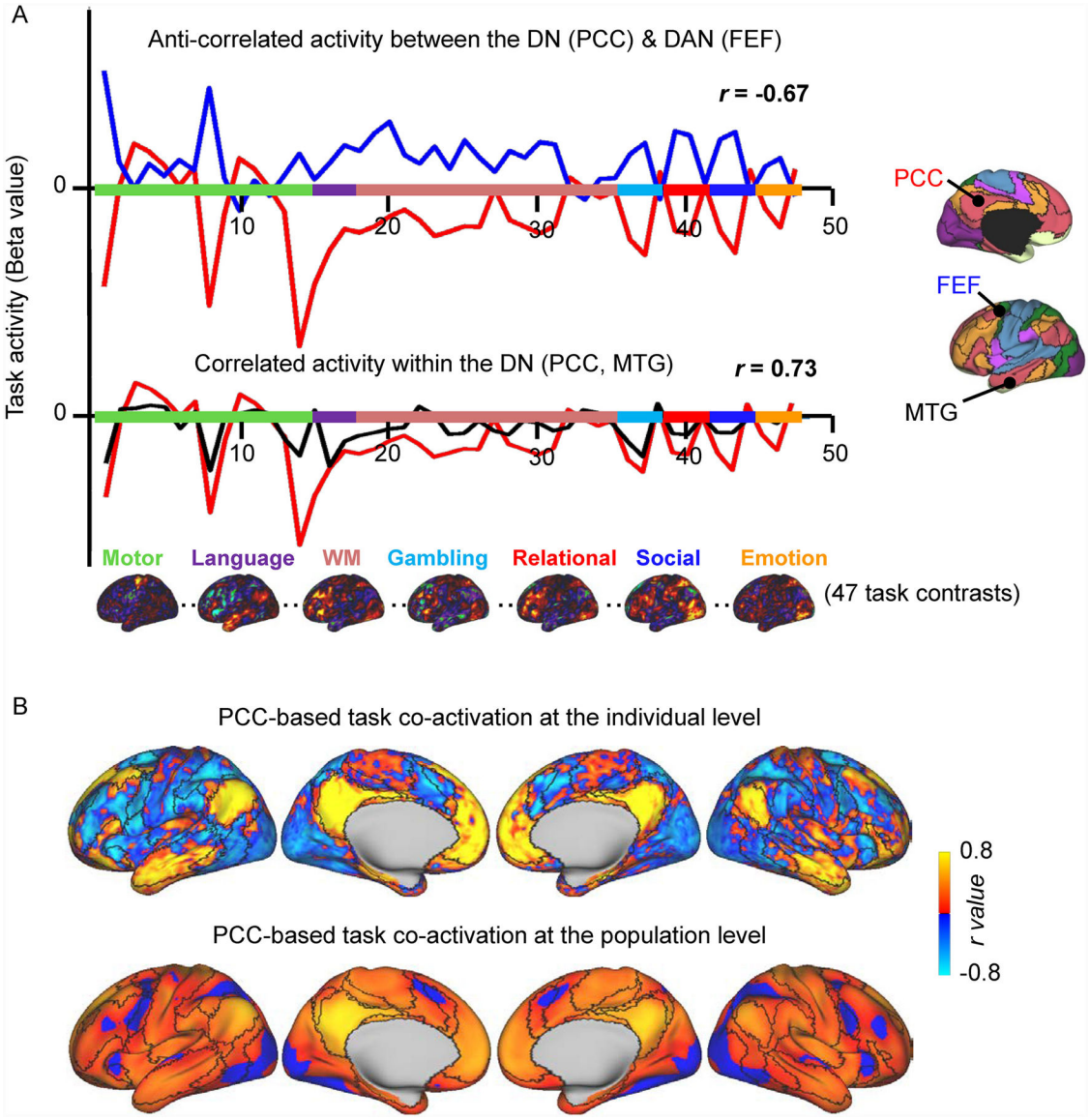


**Fig. 1. Anti-correlations are present during task performance.**

(A) Forty-seven task activation beta values across a set of task contrasts are shown for two seeds from the DN, PCC (red line) and MTG (black line), and one seed from the DAN, FEF (blue line) in one HCP participant ("748258″). The PCC shows anti-correlated activity ($r$ = −0.67) with the DAN seed (FEF) and positively correlated activity ($r$ = 0.73) with a seed (MTG) in its own network (DN). Seven activation maps from different cognitive domains projected onto the cortical surface are shown. The colors on the x axis indicate the contrasts belonging to each task. (B)Task co-activation map for a seed region in the PCC at the individual level (top) and at the population level (bottom). The task co-activation maps exhibit connections that are consistently positive and others that are consistently anti-correlated. Concordant with resting-state functional connectivity, the task-based co-activation map of the PCC shows positive correlations with other default network regions such as the MTG, and anti-correlations with DAN areas such as the FEF. The color scale

illustrates Pearson *r* coefficients, with warm colors indicating positive correlations and cool colors indicating negative correlations. The black outlines indicate network boundaries based on the parcellation detailed in Yeo et al. (2011).

DAN, dorsal attention network; DN, default network; FEF, frontal eye field; MTG, middle temporal gyrus; PCC, posterior cingulate cortex.

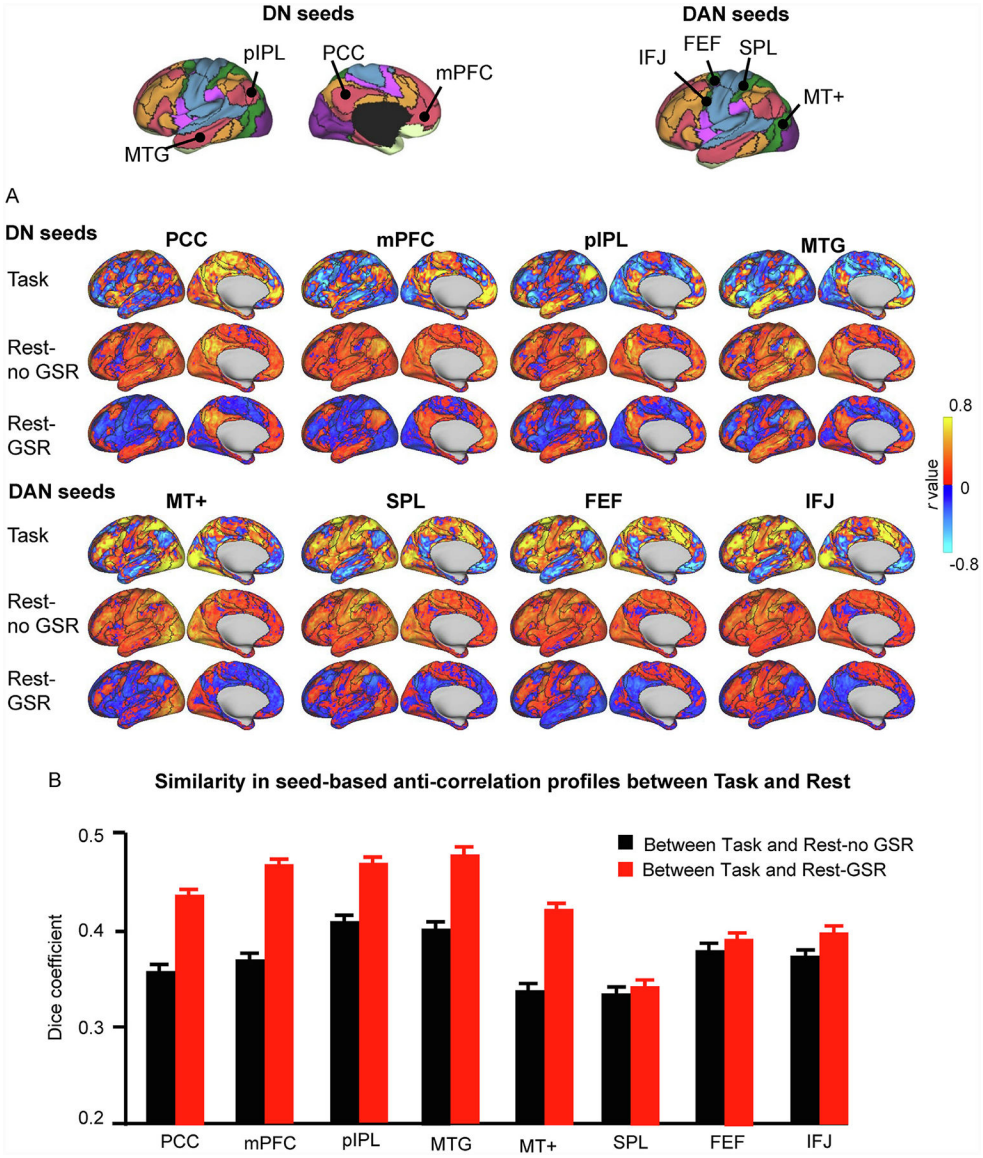


**Fig. 2. Anti-correlations are largely preserved across task and resting-state conditions.**

(A) Correlation maps from one participant ("784565″) were generated using seeds of the DN and DAN. The seeds are shown at the top of the figure, where black delineations indicate the boundaries of the 17-network parcellation and colors indicate the 7-network parcellation for easy identification of large-scale networks (Yeo et al., 2011). For each seed, we generated correlation maps (only the left cerebral hemisphere is shown) based on i) HCP task data, where task-evoked activity across the 47 task contrasts of the HCP database were concatenated (Task); ii) HCP resting-state data preprocessed without GSR (Rest-no GSR); and iii) HCP resting-state data preprocessed with GSR (Rest-GSR). The presence of anti-correlations across conditions, as well as their preserved spatial distribution, suggests that anti-correlations are meaningful and not simply spurious observations resulting from the GSR preprocessing step. The color scales illustrate *r* scores, whereby warm colors indicate positive correlations and cool colors indicate negative correlations. (B) Similarity in the

seed-based anti-correlations between the Task and Rest-no GSR conditions (black bars) and between the Task and Rest-GSR conditions (red bars) across all participants. Similarity was quantified by calculating the Dice overlap coefficient between task-based and resting-state anti-correlations for each participant, and then averaged across participants. The Dice coefficients are greater for the Rest-GSR condition than for the Rest-no GSR condition (paired *t*-test, $p<0.0001$ for all seeds except for the SPL seed). Error bars represent standard errors.

DAN, dorsal attention network; DN, default network; PCC: posterior cingulate cortex; mPFC: medial prefrontal cortex; pIPL, posterior inferior parietal lobe; MTG: middle temporal gyrus; MT+: middle temporal region; SPL: superior parietal lobule; FEF: frontal eye field; IFJ: inferior frontal junction.

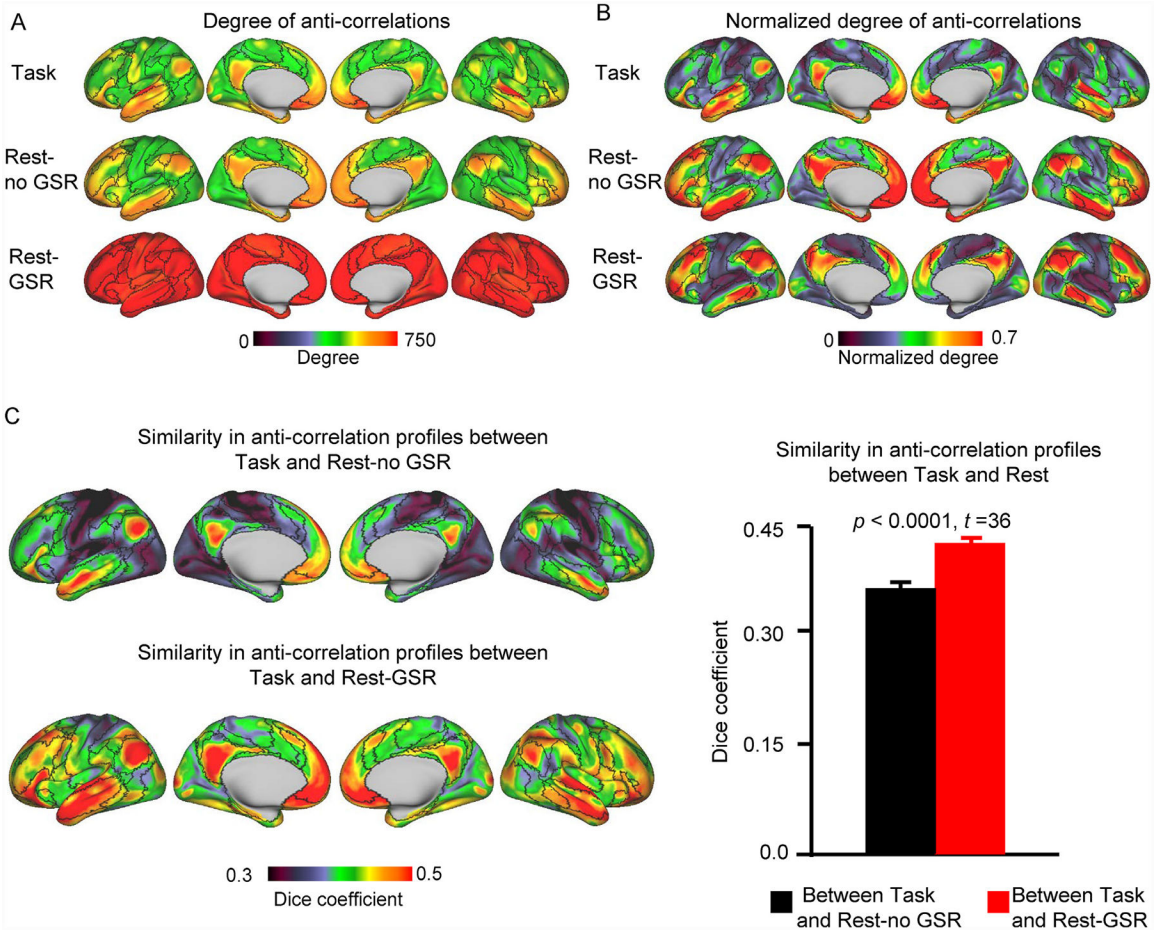


**Fig. 3. Default network areas exhibit many anti-correlations across task and resting-state conditions.**

(A) The degree of anti-correlations was mapped for every vertex on the cortical surface. It was calculated as the number of anti-correlations between a given vertex and all other 1483 vertices on the cortical surface. Maps were obtained and averaged across all 680 HCP participants. Vertices in the Rest-GSR condition show the strongest degrees of anti-correlations, followed by the Rest-no GSR condition, while the Task condition had the lowest degrees of anti-correlations. The color scale indicates the degree (number) of anti-correlations. (B) To facilite the visualization of the distribution of anti-correlations across the cortical surface, we generated maps of the normalized degree of anti-correlations for each condition. Regardless of the condition (Task, Rest-no GSR, Rest-GSR), default network and limbic network areas exhibit a higher degree of anti-correlations with the rest of the cortical surface. (C) Similarity in the anti-correlation profiles between the Task and Rest-no GSR conditions (left, top row) and between the Task and Rest-GSR conditions (left, bottom row). Similarity was quantified at each vertex by calculating the Dice overlap coefficient between task-based and resting-state anti-correlation profiles for each participant, and averaged across participants thereafter. The color scale indicates the Dice coefficient. Overall, when considering all vertices together (right), GSR-preprocessed resting-state data shows a higher similarity to task data than does resting-state data not processed with GSR (paired *t*-test: $t(679) = 36$, $p < 0.0001$). Error bars represent standard errors.

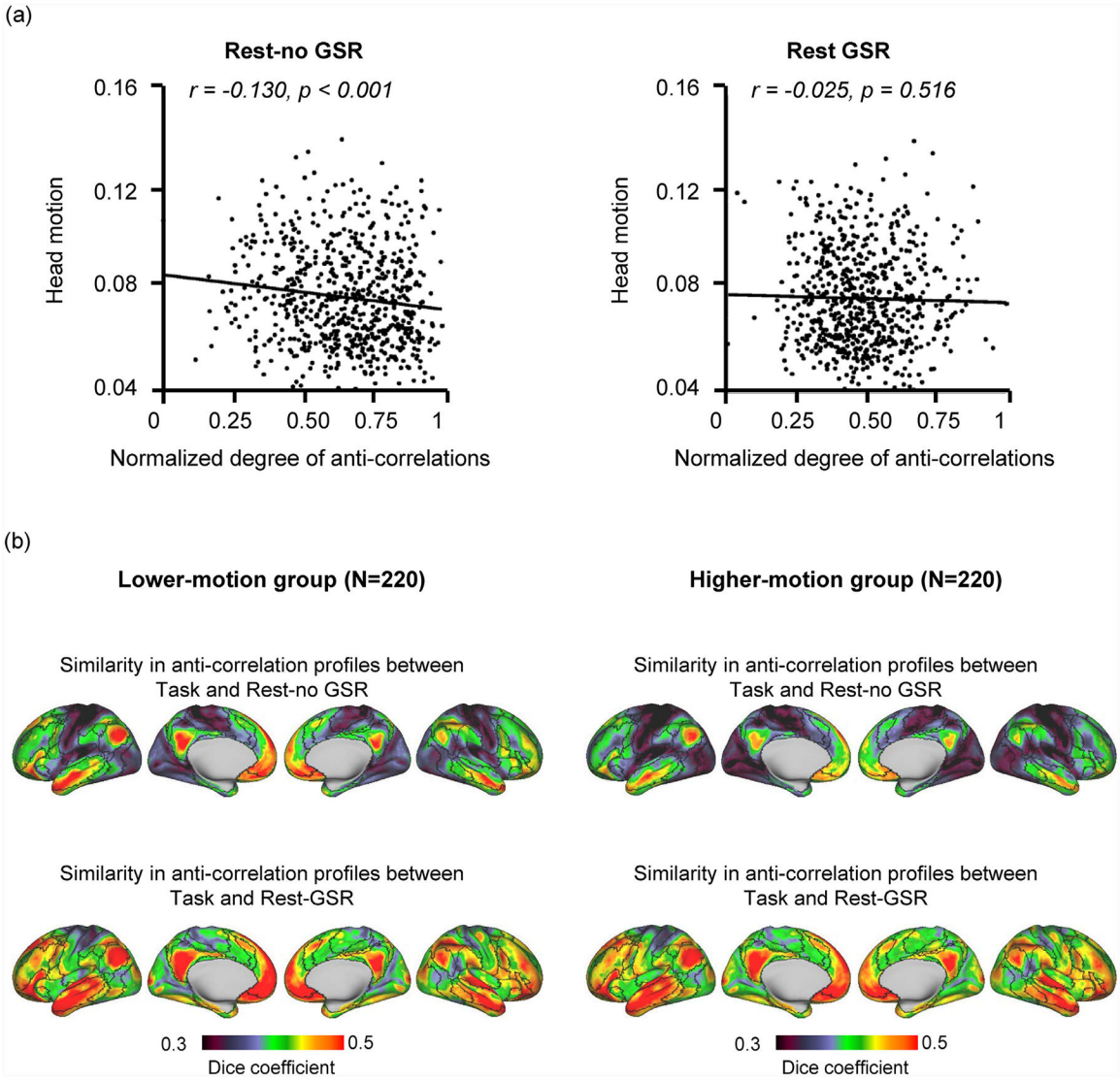


**Fig. 4. Motion effect on the anti-correlations.**

(A) Correlation between head motion and normalized degree of whole-brain anti-correlations in Rest-no GSR and Rest-GSR conditions. Motion significantly correlates with the degree of anti-correlations in Rest-no GSR condition ($r = -0.13$, $p < 0.001$), but not in Rest-GSR condition ($r = -0.025$, $p = 0.516$).The degree of whole-brain anti-correlations represents the sum of anti-correlations mapped for each vertex. (B) Similarity in the anti-correlation profiles between the Task and Rest-no GSR conditions (top row) and between the Task and Rest-GSR conditions (bottom row) was quantified in the lower-motion subgroup and the higher-motion subgroup. Anti-correlation profiles in the Task condition are more similar to those of the Rest-GSR condition than to those of the Rest-no GSR condition, in both the higher-motion group (paired *t*-test: $t(219) = 22$, $p<0.0001$) and the lower-motion groups (paired *t*-test: $t(219) = 19$, $p<0.0001$).

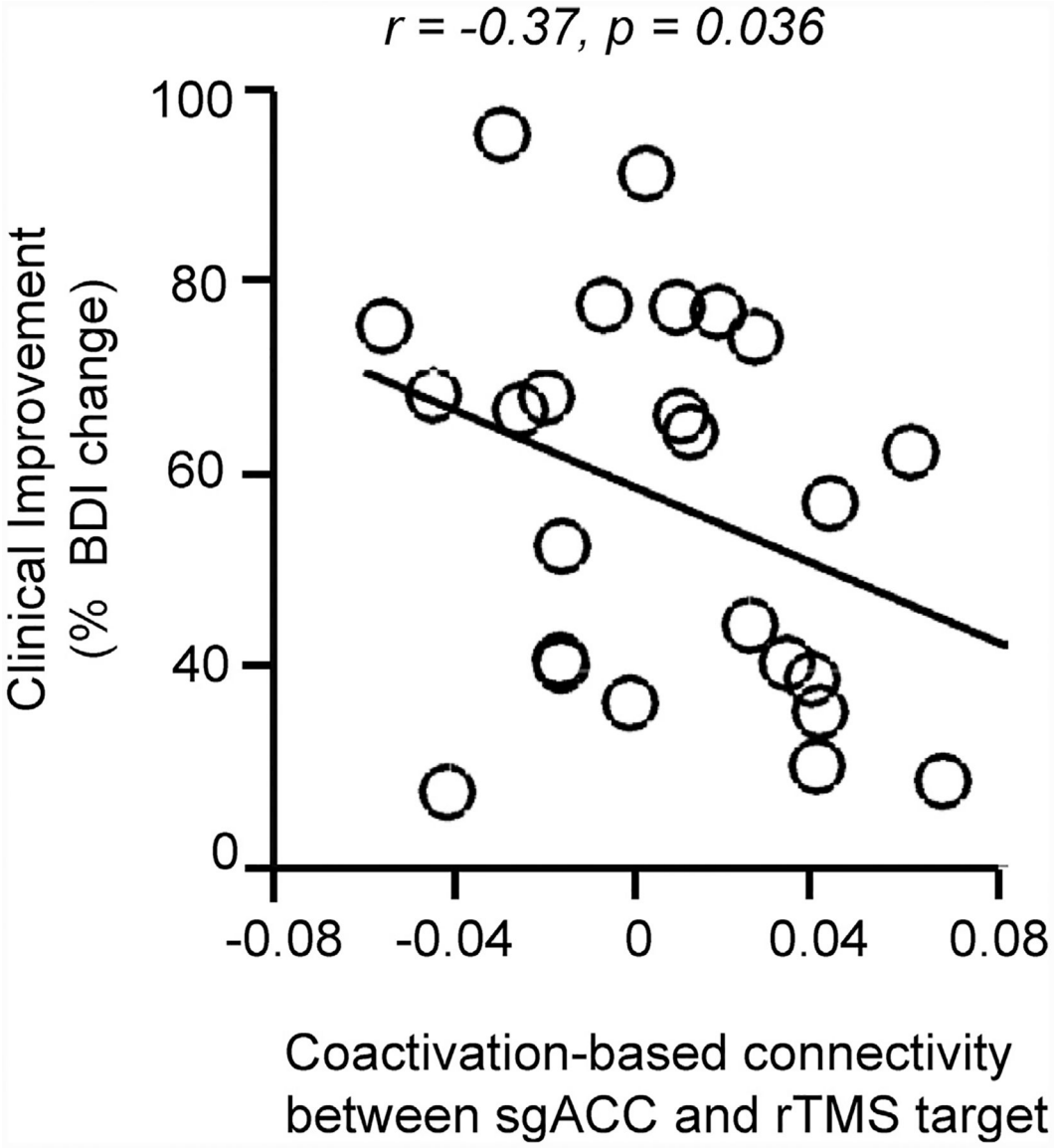


**Fig. 5. Left DLPFC rTMS sites associated with higher clinical efficacy show stronger task-based anti-correlations with the sgACC.**

We investigated whether anti-correlations can explain clinical efficacy following rTMS of various DLPFC sites in 25 patients with depression. We assessed the association between clinical efficacy (% decrease in BDI) and population-level task-based co-activation. There is a significant negative relationship between clinical efficacy and DLPFC-sgACC co-activation ($r = -0.37$, $p = 0.036$). These negative correlations indicate that the stronger the DLPFC-sgACC anti-correlation, the higher the rTMS clinical efficacy. BDI, Beck's Depression Inventory; DLPFC, dorsolateral prefrontal cortex; sgACC, subgenual anterior cingulate cortex; rTMS, repetitive transcranial magnetic stimulation.

**Table 1**

Forty-seven task contrasts included in our study from the seven fMRI HCP tasks.

| Contrast # | Task | COPE | Contrast description | Contrast # | Task | COPE | Contrast |
|---|---|---|---|---|---|---|---|
| 1 | Motor | cope1 | Cue - Fixation | 25 | | cope9 | 2-back - Fixation |
| 2 | | cope2 | Left foot - Fixation | 26 | | cope10 | 0-back - Fixation |
| 3 | | cope3 | Left hand - Fixation | 27 | | cope11 | 2-back - 0-back |
| 4 | | cope4 | Right foot - Fixation | 28 | | cope15 | Body - Fixation |
| 5 | | cope5 | Right hand - Fixation | 29 | | cope16 | Face - Fixation |
| 6 | | cope6 | Tongue - Fixation | 30 | | cope17 | Place - Fixation |
| 7 | | cope7 | Average - Fixation | 31 | | cope18 | Tool - Fixation |
| 8 | | cope8 | Cue - Average * | 32 | | cope19 | Body - Average |
| 9 | | cope9 | Left foot - Average | 33 | | cope20 | Face - Average |
| 10 | | cope10 | Left hand - Average | 34 | | cope21 | Place - Average |
| 11 | | cope11 | Right foot - Average | 35 | | cope22 | Tool - Average |
| 12 | | cope12 | Right hand - Average | 36 | Gambling | cope1 | Punish - Fixation |
| 13 | | cope13 | Tongue - Average | 37 | | cope2 | Reward - Fixation |
| 14 | Language | cope1 | Math - GLM intercept | 38 | | cope3 | Punish - Reward |
| 15 | | cope2 | Story - GLM intercept | 39 | Relational | cope1 | Match - Fixation |
| 16 | | cope3 | Math - Story | 40 | | cope2 | Relational - Fixation |
| 17 | WM | cope1 | 2-back body - Fixation | 41 | | cope3 | Match - Relational |
| 18 | | cope2 | 2-back face - Fixation | 42 | Social | cope1 | Random - Fixation |
| 19 | | cope3 | 2-back place - Fixation | 43 | | cope2 | ToM - Fixation |
| 20 | | cope4 | 2-back tool - Fixation | 44 | | cope3 | Random - ToM |
| 21 | | cope5 | 0-back body - Fixation | 45 | Emotion | cope1 | Faces - GLM intercept |
| 22 | | cope6 | 0-back face - Fixation | 46 | | cope2 | Shapes - GLM intercept |
| 23 | | cope7 | 0-back place - Fixation | 47 | | cope3 | Faces - Shapes |
| 24 | | cope8 | 0-back tool - Fixation | | | | |

* Average represents the beta map for all task-specific experimental conditions combined.COPE: contrast of parameter estimate (identifier for HCP contrasts); ToM: Theory of Mind; WM: Working Memory.